Supporting Information

Hidden Isomer of Trifluoroacetylacetone Revealed by Matrix Isolation Infrared and Raman Spectroscopy

Alejandro Gutiérrez-Quintanilla,[a,b †] Rasa Platakyte,[c] Michèle Chevalier,[a] Claudine Crépin,[a*] Justinas Ceponkus[c*]

[a]Université Paris-Saclay, CNRS, Institut des Sciences Moléculaires d'Orsay, 91405, Orsay, France.
[b]Instituto Superior de Tecnologías y Ciencias Aplicadas (InSTEC), Universidad de La Habana. Ave. Salvador Allende No. 1110, Quinta de los Molinos, La Habana 10400, Cuba.
[c]Institute of Chemical Physics, Vilnius University, Sauletekio av. 9, L-10222 Vilnius, Lithuania.
† Present address: Aix-Marseille Université, Laboratoire PIIM, Team ASTRO, Service 252, Saint Jérôme, Ave. Escadrille Normandie Niemen, 13013 Marseille, France.

Corresponding authors: claudine.crepin-gilbert@universite-paris-saclay.fr; justinas.ceponkus@ff.vu.lt

Content:

I. Geometries

Figure S1: *Geometries of the keto isomer (top, middle) and the different enolic structures of TFacac. Isomer **1** (left) and isomer **2** (right), with their labels*

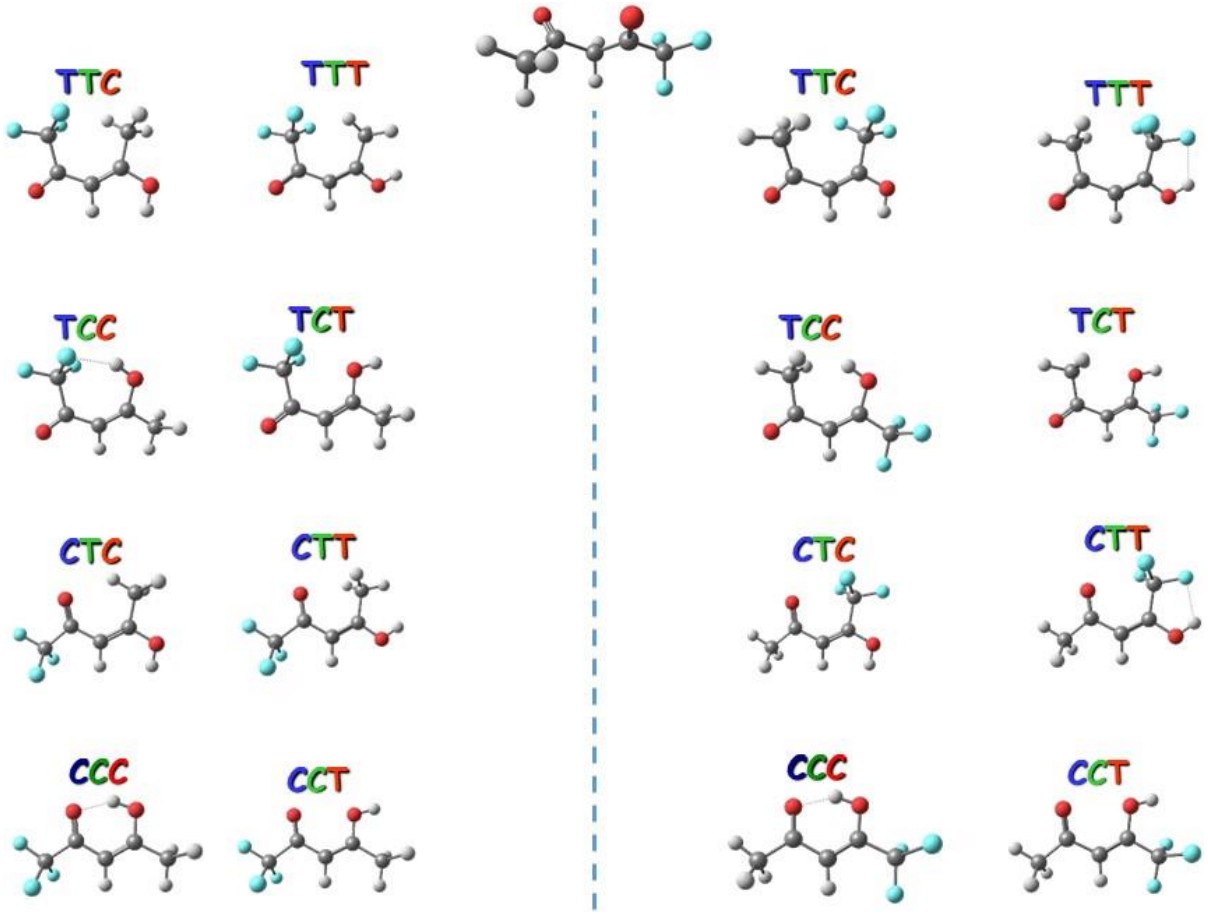

Table S1: Geometries of the two chelated enol isomers of TFacac obtained by *ab initio* MP2, DFT/M06-2X and DFT/B3LYP-D3 calculations with the 6-311++G(3df,3pd) basis set. Main distances R in Å, angles A and dihedral angles D in degrees.

isomer 1 - CCC(CO)

	MP2	M06-2X	B3LYP-D3
R(1-2)	1.340	1.335	1.347
R(1-3)	1.340	1.335	1.348
R(1-4)	1.321	1.317	1.328
R(1-5)	1.539	1.544	1.552
R(5-6)	1.426	1.43	1.425
R(5-13)	1.237	1.221	1.231
R(6-7)	1.077	1.077	1.077
R(6-8)	1.37	1.364	1.371
R(8-9)	1.486	1.488	1.489
R(8-14)	1.321	1.315	1.319
R(9-10)	1.089	1.09	1.091
R(9-11)	1.089	1.09	1.091
R(9-12)	1.085	1.085	1.086
R(14-15)	0.994	0.986	0.994
R(13-15)	1.655	1.709	1.693
A(2-1-3)	107.5	107.4	107.3
A(2-1-4)	108.5	108.5	108.2
A(2-1-5)	110.1	110.2	111.1
A(3-1-4)	108.5	108.5	108.3
A(3-1-5)	110.1	110.2	109.6
A(4-1-5)	112	112	112.1
A(1-5-6)	116.3	115.9	116.7
A(1-5-13)	118.6	118.3	118
A(6-5-13)	125.1	125.7	125.3
A(5-6-7)	120.5	120.2	120.2
A(5-6-8)	119.5	119.5	119.9
A(5-13-15)	98	98.4	98.5
A(7-6-8)	120	120.3	120
A(6-8-9)	124.1	123.9	124
A(6-8-14)	122	122.5	122.1
A(9-8-14)	113.9	113.6	113.8
A(8-9-10)	109.3	109.1	109.4
A(8-9-11)	109.3	109.1	109.4
A(8-9-12)	111.3	111.4	111.7
A(8-14-15)	106.4	108.3	107.7
A(10-9-11)	107.6	107.5	107.2
A(10-9-12)	109.6	109.8	109.5
A(11-9-12)	109.6	109.8	109.5
A(14-15-13)	149.1	145.5	146.5
D(4-1-5-13)	0	0	18.0
D(3-1-5-13)	120.8	120.8	102.4
D(1-5-6-8)	180	180	177.5
D(5-6-8-9)	180	180	179.6
D(12-9-8-14)	180	180	180.0
D(11-9-8-14)	58.8	58.6	58.6
D(9-8-14-15)	180	180	180
D(5-13-15-14)	0	0	0
D(1-5-6-7)	0	0	2.5

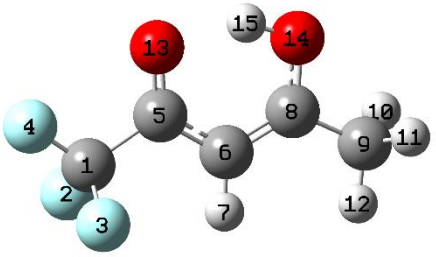

isomer 2 - CCC(OH)

	MP2	M06-2X	B3LYP-D3
R(1-2)	1.090	1.090	1.092
R(1-3)	1.090	1.090	1.092
R(1-4)	1.085	1.085	1.086
R(1-5)	1.500	1.501	1.504
R(5-6)	1.452	1.459	1.454
R(5-13)	1.241	1.227	1.237
R(6-7)	1.077	1.077	1.077
R(6-8)	1.357	1.346	1.353
R(8-9)	1.513	1.517	1.522
R(8-14)	1.317	1.312	1.316
R(9-10)	1.333	1.329	1.341
R(9-11)	1.333	1.329	1.341
R(9-12)	1.334	1.33	1.341
R(14-15)	1.002	0.994	1.002
R(13-15)	1.614	1.659	1.65
A(2-1-3)	107.4	107.3	107
A(2-1-4)	110.0	110.2	109.9
A(2-1-5)	109.7	109.6	110
A(3-1-4)	110.0	110.2	109.9
A(3-1-5)	109.7	109.6	110
A(4-1-5)	110.1	110.0	110.1
A(1-5-6)	118.2	117.9	118.2
A(1-5-13)	120.9	121.1	120.8
A(6-5-13)	120.9	121.1	121
A(5-6-7)	121.0	120.8	120.6
A(5-6-8)	119.0	118.9	119.4
A(5-13-15)	101.9	102.7	102.3
A(7-6-8)	120.0	120.3	120
A(6-8-9)	122.9	122.5	122.7
A(6-8-14)	124.8	125.6	125
A(9-8-14)	112.3	111.8	112.3
A(8-9-10)	110.6	110.6	110.7
A(8-9-11)	110.6	110.6	110.7
A(8-9-12)	111.4	111.5	111.7
A(8-14-15)	104.3	106.0	105.6
A(10-9-11)	108.0	107.9	107.8
A(10-9-12)	108.1	108.0	107.9
A(11-9-12)	108.1	108.0	107.9
A(14-15-13)	149.2	145.7	146.7
D(4-1-5-13)	0	0	0
D(3-1-5-13)	121.2	121.3	121.2
D(1-5-6-8)	180	180	180
D(5-6-8-9)	180	180	180
D(12-9-8-14)	180	180	180
D(11-9-8-14)	59.8	59.7	59.8
D(9-8-14-15)	180	180	180
D(5-13-15-14)	0	0	0
D(1-5-6-7)	0	0	0

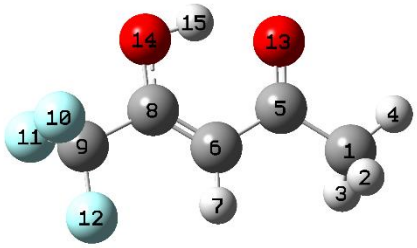

II. Torsional barriers in CCC(OH)

Figure S2: Relaxed torsional barriers for CF_3 and CH_3 groups in the CCC(OH) isomer obtained at the MP2(FC)/ 6-311++G(3df,3pd) level of theory. An Akima interpolation spline is used as a guide for the eye.

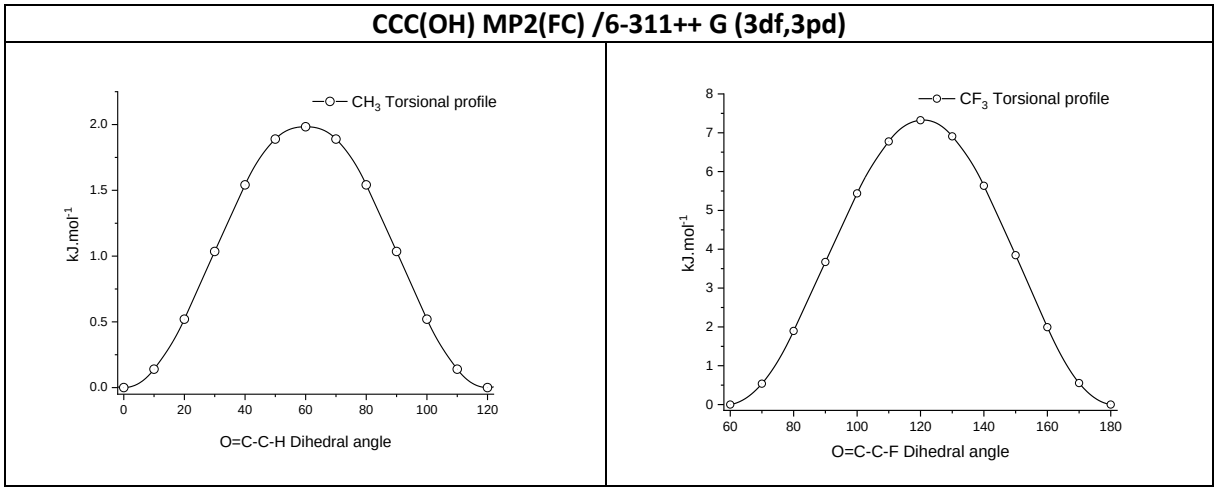

III. Correlations between mode frequencies calculated with the three methods

Calculations were performed at three levels of theory: MP2(FC)/ 6-311++G(3df,3pd) [MP2], DFT/M06-2X/ 6-311++G(3df,3pd) [M06-2X] and DFT/B3LYP-D3/6-311++G(3df,3pd) [B3LYP-D3]. Figures S2 and S3 show plots of mode frequencies obtained with one method versus frequencies obtained with the other methods, for CCC(CO) and CCC(OH) respectively. All values in cm^{-1}. Red lines correspond to linear fits including the (0,0) point.

Figure S3: CCC(CO)

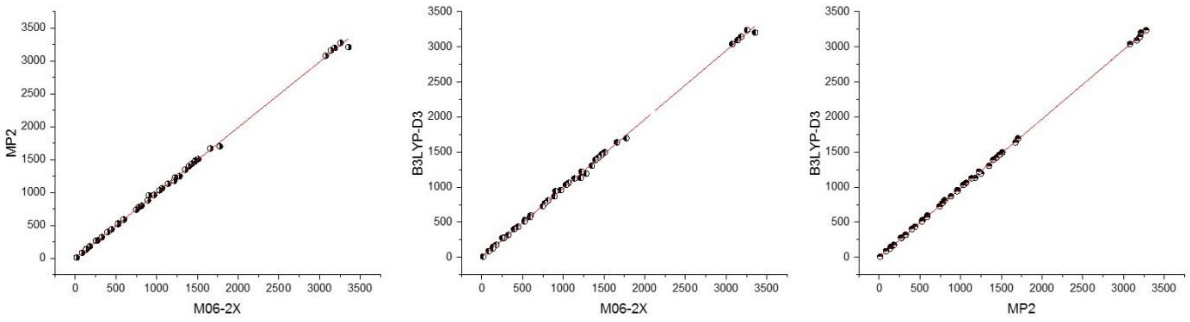

Figure S4: CCC(OH)

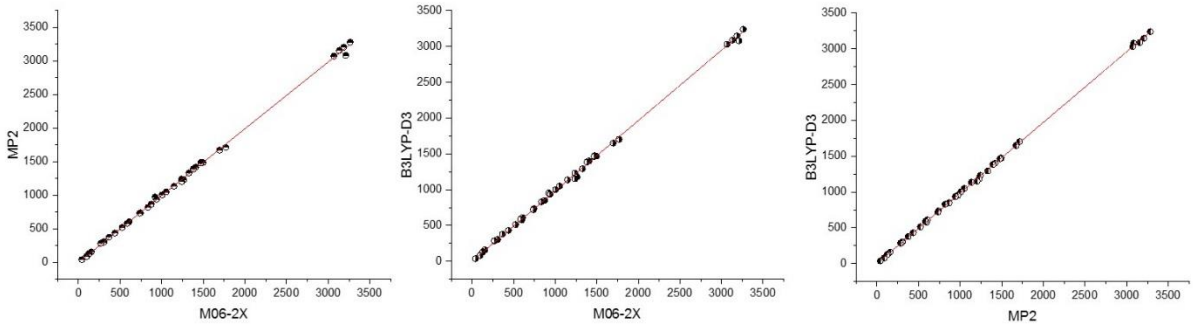

The results of the linear fits are very similar for both isomers:

ν(B3LYP-D3)=0.983*ν(M06-2X)=0.986*ν(MP2) for CCC(CO)

ν(B3LYP-D3)=0.983*ν(M06-2X)=0.987*ν(MP2) for CCC(OH)

The best correlation is obtained between MP2 and DFT/B3LYP-D3 for both isomers. The main mismatches with M06-2X results concern the OH modes and especially the OH stretching mode, the out-of-phase C=C/C=O stretching mode and the CF stretching modes. The correlations are much better for the CCC(OH) isomer than for the CCC(CO) isomer. This could be linked to the difficulties to get a reliable geometry for the CCC(CO) isomer (see main text).

IV. Spectra in nitrogen matrices: band assignments to CCC(CO) and CCC(OH)

Figure S5: Spectrum of trifluoroacetylacetone in nitrogen matrix: after deposition (violet), after successive UV irradiation (grey), difference spectrum (red), 9 K after 30 K annealing (after irradiation) (green), difference spectrum (blue), and difference from another annealing (without irradiation of the sample) (pink).

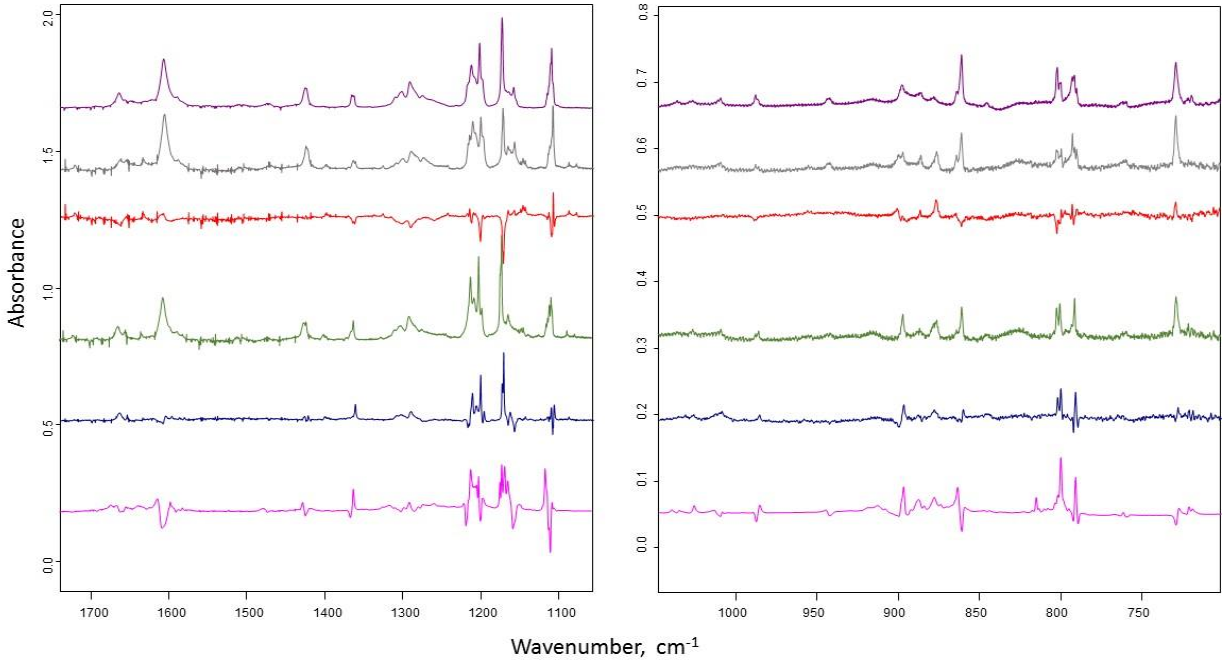

Figure S6: IR spectra of CCC(CO) - top - and CCC(OH) - bottom – in nitrogen matrix extracted from IR spectra recorded before and after irradiation and before and after annealing of the sample.

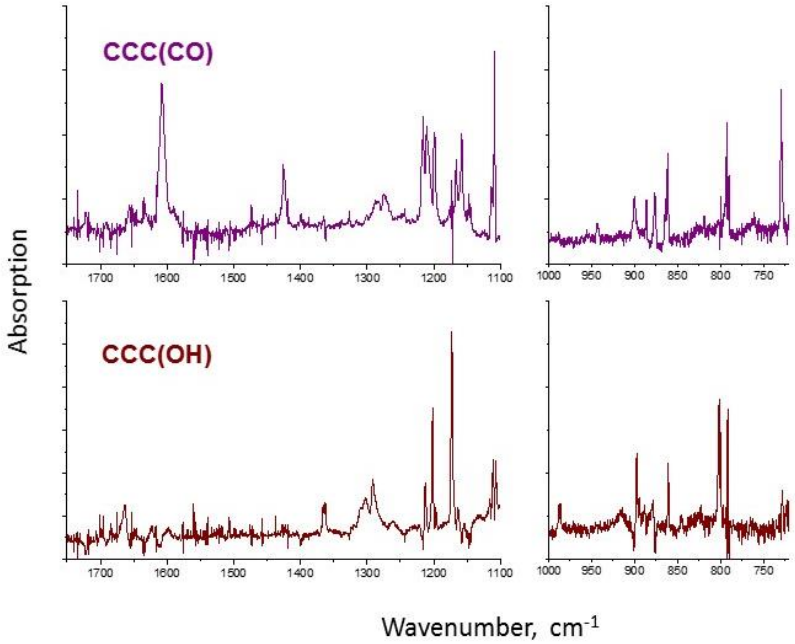

Figure S7: IR (top) and Raman (bottom) spectra of TFacac in nitrogen matrices (black curves) with M06-2X predictions of IR and Raman intensities for CCC(CO) (red) and CCC(OH) (blue) [theoretical Raman intensities are obtained from Raman activities with the use of an excitation wavelength of 785 nm]

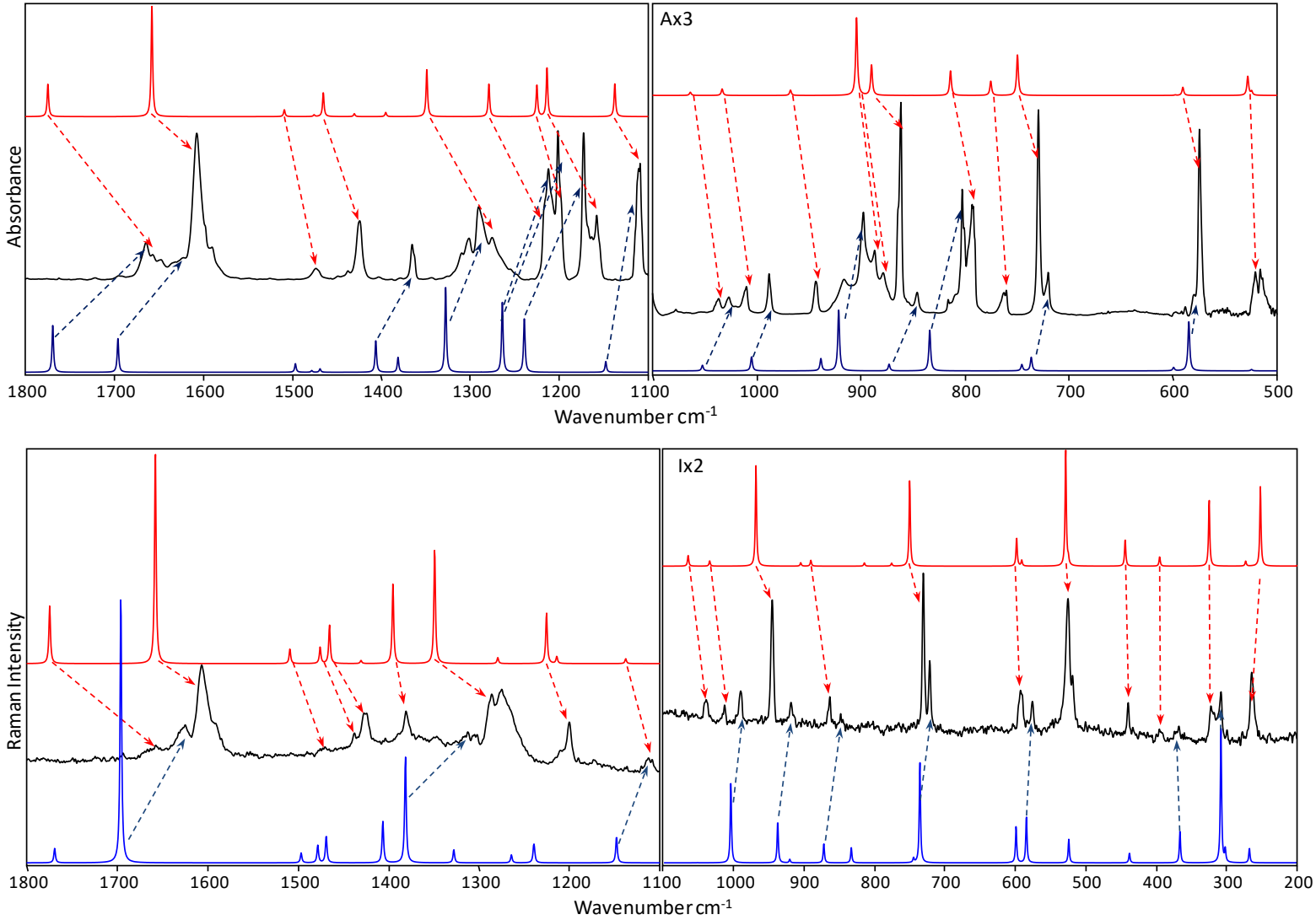

V. Comparison between theoretical and experimental mode frequencies

The comparison between the three methods (Part III of SI) shows some problems in the description of OH modes and CF_3 stretching modes. We focus the comparison on the 700-1500 cm^{-1} spectral range, i.e. modes 8 to 25 (see Tables 2 and 3), including these CF_3 modes and OH bending modes. The comparison with experiments does not bring very reliable data concerning the OH modes in CCC(CO) because of the structure and the broadness of the experimental bands.

In order to check which method describes TFacac in the best way, we performed averages of ν(exp)/ν(theo) ratio between experimental frequencies and theoretically predicted frequencies, in the spectral range under study, with and without CF_3 and OH modes. Scaling factors (sf) are obtained for the three methods and the dispersion of the values indicate the accuracy of the method. Three matrices were especially explored: Ne, *p*H_2 (giving values close to the gas phase), and N_2 (with the largest amount of experimental values when combining Raman and IR results). Results in N_2 are detailed in the main text. Figure S8 shows these frequency ratios (ν(exp)/ν(theo)) in the spectral range of interest for both isomers, in Ne and *p*H_2 matrices and in the three levels of theory: *ab initio* MP2(FC)/6-311++G(3df,3pd) ("MP2"), DFT M06-2X//6-311++G(3df,3pd) ("M06-2X") and DFT B3LYP-D3//6-311++G(3df,3pd) ("B3LYP"). When excluding CF_3 and OH modes (in green and red rectangles in Figure S8 respectively), ν(exp)/ν(theo) values are almost constant with the three methods, indicating that the use of a scaling factor makes sense in this spectral range, at least for the CCC(CO) isomer. There are not enough values for CCC(OH) in Ne and *p*H_2 to conclude, but the same remark is valid with values in N_2 for both isomers. One can notice that the dispersion of the ratio values is larger with the B3LYP method than with the other two methods. More precisely, the best method to describe the molecule when excluding CF_3 and OH modes (less dispersion) is found to be M06-2X. One can see in Figure S8 that values related to CF_3 modes are well aligned using the MP2 method (black squares). M06-2X remains better than B3LYP when including the CF_3 modes. Finally, the dispersion remains the smallest using the M06-2X method when including all the modes, but MP2 gives a very good description of the modes. The averaging process was performed in three steps: (i) including all the modes except OH and CF_3 modes, (ii) including all the modes excluding the OH modes, and (iii) including all the bands of the spectral range. Scaling factors obtained in the three steps are reported in Table S2. The comparison between the three steps clearly shows the influence of CF_3 modes and OH bending modes and the accuracy of the methods to calculate these modes. The variations of the scaling factors from one matrix to another, or from one isomer to the other are weak. Figure 7 is obtained using a "global" scaling factor: 0.970 for MP2, 0.971 for M06-2X, and 0.985 for B3LYP. One can remark that the scaling factors for MP2 and M06-2X are very close, in agreement with the results of Part III concerning the comparison between theoretical models.

Additional remark: Several experimental bands are not assigned (Tables 4 and 5), there is a possibility that they appear because of vibrational resonances between one mode and combinations or overtones of other modes. Tentative assignments can be checked using graphs such as those of Figure S8, looking at the agreement with the scaled M06-2X or MP2 values which seem quite reliable. We performed this kind of test with the additional bands in the range of CF stretching bands: no clear conclusion arises. In contrast, mode 12 could appear as two bands in the Raman spectra of both isomers. In fact, the two values are below and above the predicted scaled value. We have thus taken into account both values in the analysis of data in nitrogen matrices (Figure 7).

Figure S8: ν(exp)/ν(theo) values for the various modes included in the 700-1500 cm^{-1} spectral range; CCC(CO) left panels, CCC(OH) right panels, in Ne (top panels), in pH_2 (bottom panels); black squares MP2, red circles M06-2X, blue triangles B3LYP; modes involving OH bending underlined by red vertical strips (modes 13 and 21 in CCC(CO), 13 and 20 in CCC(OH)) and CF_3 modes underlined by green vertical strips (modes 14 and 16 in CCC(CO), 15 and 16 in CCC(OH)).

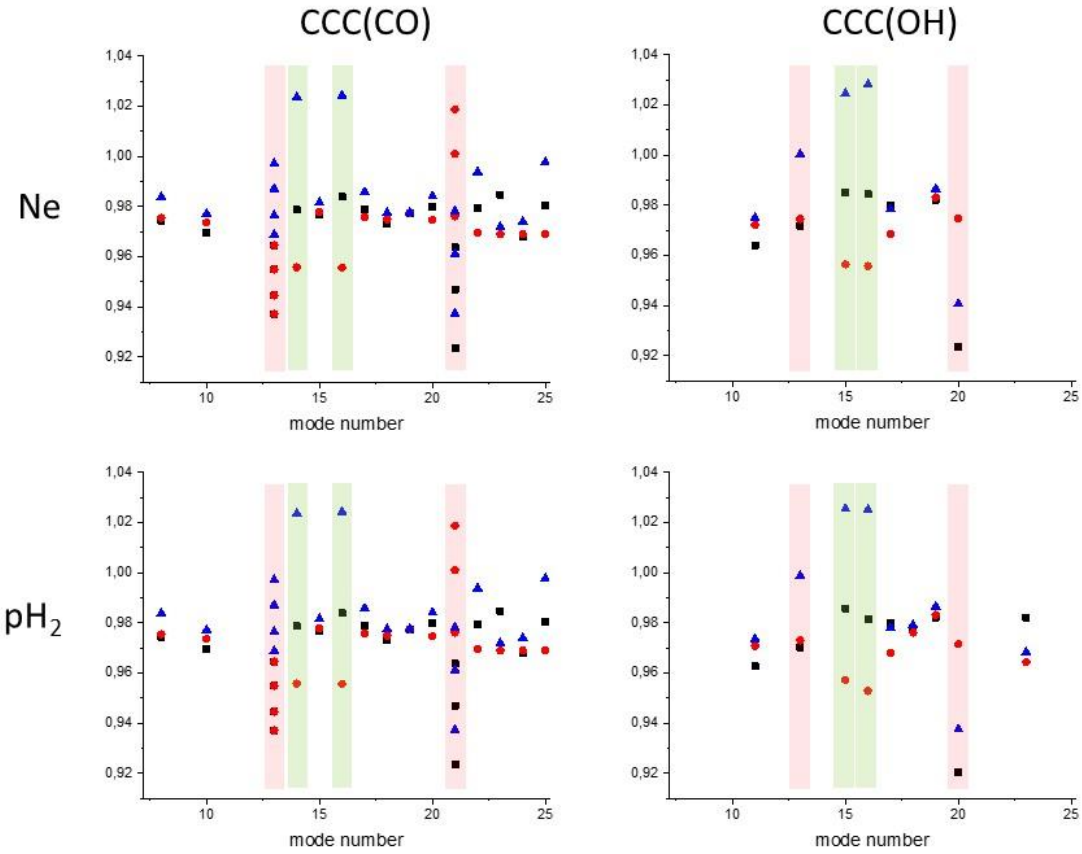

Table S2: Scaling factors obtained in the three steps described in the text, reported as (i), (ii) and (iii), in the 700-1500 cm^{-1} range of mode frequencies with experimental data in N_2, Ne and pH_2. Values in parenthesis are errors on the last digits.

	MP2			**M06-2X**			**B3LYP**		
CCC(CO)	N_2	Ne	pH_2	N_2	Ne	pH_2	N_2	Ne	pH_2
(i)	0.9772 (20)	0.9798 (18)	0.9766 (15)	0.9757 (17)	0.9765 (11)	0.9733 (11)	0.9836 (23)	0.9855 (20)	0.9823 (24)
(ii)	0.9772 (10)	0.9802 (15)	0.9674 (14)	0.9725 (26)	0.9734 (22)	0.9706 (20)	0.9881 (37)	0.9916 (40)	0.9888 (47)
(iii)	0.9684 (39)	0.9699 (40)	0.9671 (38)	0.9722 (32)	0.9709 (37)	0.9708 (40)	0.9826 (42)	0.9859 (44)	0.9830 (43)
CCC(OH)									
(i)	0.9757 (46)	0.9755 (57)	0.9770 (37)	0.9741 (46)	0.9746 (44)	0.9725 (33)	0.9808 (53)	0.9800 (34)	0.9771 (30)
(ii)	0.9767 (36)	0.9792 (39)	0.9789 (28)	0.9690 (45)	0.9672 (51)	0.9676 (40)	0.9901 (64)	0.9986 (115)	0.9909 (91)
(iii)	0.9731 (44)	0.9702 (83)	0.9714 (68)	0.9704 (37)	0.9642 (40)	0.9686 (31)	0.9887 (62)	0.9906 (115)	0.9859 (93)